

Analog charged black hole formation via percolation: Exploring cosmic censorship and Hoop conjecture

Nitesh Jaiswal^{1,*} and S. Shankaranarayanan^{1,†}

¹*Department of Physics, Indian Institute of Technology Bombay, Mumbai 400076, India*

Abstract

We investigate an analog model of charged black hole (BH) formation using the framework of classical percolation. By analyzing the scaling behavior of key quantities, including surface gravity and Komar mass, we establish a robust correspondence between this analog system and gravitational collapse in general relativity. Our numerical simulations of the lattice model show excellent agreement with analytical predictions for the continuum limit, highlighting the potential of analog systems to capture essential features of BH physics. Interestingly, we find that while geometric criteria related to the hoop conjecture are necessary, they are not sufficient for BH formation in our model. Instead, the exponential growth of energy and cluster size emerges as the key indicator, suggesting a novel interpretation of the hoop conjecture and providing further support for cosmic censorship within our analog framework by ensuring horizon formation. This work offers a fresh perspective on the organization of matter within BH event horizons and lays the groundwork for future quantum extensions that could shed light on Hawking radiation and the BH information paradox by linking entanglement entropy in quantum percolation models to BH entropy.

* niteshphy@iitb.ac.in

† shanki@iitb.ac.in

I. INTRODUCTION

Black holes (BHs) pose a challenge to our understanding of the fundamental laws of physics [1–3]. The BH information paradox, stemming from the apparent conflict between quantum mechanical unitarity and the seemingly irreversible nature of BH evaporation [2, 3], highlights a critical gap in our knowledge. This paradox hinges critically on our understanding of the nature of singularities [4] and their fate in quantum gravity [5–12]. The cosmic censorship hypothesis, if true, suggests that these singularities are always cloaked by event horizons, further complicating the question of how information might escape [13]. While a complete theory of quantum gravity is expected to provide the ultimate resolution [14], its development remains a formidable challenge. A central question is whether the paradox can be resolved *without* a full understanding of singularities [15–18].

Condensed matter systems provide a fertile ground for exploring this enigma. These systems exhibit phenomena remarkably analogous to BHs, including quasiparticle emergence, topological phase transitions, and complex entanglement dynamics [19–29]. For instance, the emergence of quasiparticles from collective behavior mirrors Hawking radiation from a BH horizon [30–41]. By studying these systems, we can explore how information is processed in strongly correlated systems [42–45], gaining insights into the mechanisms of information preservation and loss [46–51]. While these systems are BH *analogs*, not exact replicas, they provide valuable experimental platforms for testing theoretical ideas and deepening our understanding of BHs [52–57].

Hawking radiation analogs in condensed matter differ from black holes in system size and the applicability of field-theoretic approximations. Furthermore, while the cosmic censorship hypothesis suggests that event horizons hide singularities in BHs, the absence of such horizons in analog systems raises questions about their ability to capture BH behavior fully. Therefore, assessing these analogs requires addressing key questions: When can a system mimic black hole geometry? How does a ground state evolve and reach a thermal steady state? What are the relevant timescales governing these processes?

In this work, we introduce a 1-D chiral quantum spin-chain model to explore key aspects of BH formation. The spin chain Hamiltonian, comprising N spins with non-uniform interactions, features two competing terms: an inhomogeneous, short-range non-chiral term that sets the condition for BH-like formation and a homogeneous chirality operator with next-

nearest-neighbor (NNN) interactions inducing long-range order. The interplay between these terms drives quantum phase transition (QPT) [58].

Chirality plays a crucial role in condensed matter physics, as exemplified by the chiral magnetic effect in Weyl semimetals[59–61]. In our model, the chiral term induces an imbalance in spin excitations, analogous to the charge imbalance in the chiral magnetic effect, which, in conjunction with the inhomogeneities of the non-chiral term, drives the system toward a topological QPT [58]. Chiral spin-chain models are also relevant to understanding non-perturbative phenomena in quantum field theory via lattice techniques [62, 63]. However, lattice formulations of chiral theories face the challenge of fermion doubling, as dictated by the Nielsen-Ninomiya theorem [64].

By incorporating NNN interactions, our model effectively circumvents the doubling problem. The NNN interacting chiral term ($\chi_j = \vec{\sigma}_j \cdot (\vec{\sigma}_{j+1} \times \vec{\sigma}_{j+2})$) acts as a long-range interaction, despite being constructed from local terms. This arises because the chirality operator effectively couples spins across multiple lattice sites, creating long-range correlations. The expectation value of the chirality operator, $\langle \chi_j \rangle$, encodes information about the system’s global topology [65–67]. These long-range correlations bypass Nielsen-Ninomiya theorem [64].

The formation of BHs has been linked to critical phenomena, exhibiting power-law scaling near the threshold of BH formation, analogous to phase transitions, where fluctuations occur at all length scales due to the divergence of the correlation length [68]. This work offers a novel perspective, connecting BH formation to percolation theory, a powerful framework for understanding cluster formation and connectivity at criticality, where large-scale connectivity emerges, modeling diverse physical phenomena [69]. The key idea is when matter collapses under gravity, fluctuations occur at different length scales leading to regions of varying energy density. When both the density of the collapsing region and the number of connected clusters surpass a critical threshold, these regions percolate, leading to the formation of an event horizon. Specifically, we demonstrate a correspondence between the percolation threshold in a spin chain model [69, 70] and the emergence of an event horizon-like boundary, defined by NNN-dominated regions (interior) versus nearest-neighbor (NN)-dominated regions (exterior). Within the NNN-dominated regime, we observe exponential growth in both interconnected spin clusters (analogous to matter aggregation) and the energy density within these clusters (akin to BH formation). Furthermore, we find that

the critical exponents associated with the total cluster energy and the percolation correlation length correspond to the BH mass and surface gravity exponents, respectively. We discuss the implications for cosmic censorship and the hoop conjecture.

II. CHIRAL SPIN CHAIN

The Hamiltonian of the 1-D chiral spin chain (with $\hbar = 1$) is:

$$\tilde{H} = - \sum_{j,k=1}^N \frac{U(j,k)}{2} (\sigma_j^x \sigma_k^x + \sigma_j^y \sigma_k^y) + \sum_{j=1}^N \frac{v V(j,j+2)}{4} \chi_j, \quad (1)$$

where $\vec{\sigma}_j = (\sigma_j^x, \sigma_j^y, \sigma_j^z)$ denotes the Pauli matrix vector operator of the j -th site with periodic boundary conditions (PBC) ($\vec{\sigma}_j = \vec{\sigma}_{j+N}$), $\chi_j = \vec{\sigma}_j \cdot (\vec{\sigma}_{j+1} \times \vec{\sigma}_{j+2})$ is the chirality operator [66, 67, 71–74], v is a *dimensionless constant*, $U(j,k)$ and $V(j,j+2)$ are site-dependent coupling constants that introduce inhomogeneity. The first term in the RHS describes an inhomogeneous spin-1/2 XX interaction between sites j and k , while the second term represents NNN three-spin chiral interaction involving spins at sites j , $j+1$, and $j+2$ [67]. As we show, the physical properties of the system are determined by the relative strength of the two coupling constants $U(j,k)$ and $V(j,j+2)$. We now rewrite the above Hamiltonian:

$$\tilde{H} = \sum_{j,k=1}^N V(j,j+2) H(j,k), \quad (2)$$

$$H(j,k) = -u(j,k) (\sigma_j^x \sigma_k^x + \sigma_j^y \sigma_k^y) / 2 + v \chi_j / 4, \quad (3)$$

where $u(j,k) = U(j,k)/V(j,j+2)$ is dimensionless. Since the system is 1-D, the coupling depends only on the distance between the sites, i.e., $u(j,k) \equiv u(|j-k|)$. If $V(j,j+2)$ is well-defined for all j , the key properties of the system are governed by the reduced Hamiltonian $H(j,k)$ while $V(j,j+2)$ scales the energy of the system. As shown in Appendix B, $V(j,j+2)$ is a conformal factor in the continuum limit to the spatial part of the formed BH metric [75]. Hence, Hamiltonian (1) reduces to the *dimensionless Hamiltonian*:

$$H = \sum_{j,k=1}^N H(j,k), \quad (4)$$

where j, k are now *identified as NN sites* and the coupling $u(|j-k|)$ makes the system inhomogeneous. The Hamiltonian (4), while inhomogeneous, exhibits translational invariance

since $u(|j - k|)$ depends solely on the distance between sites. A Jordan-Wigner transformation [76, 77] yields a Hamiltonian with four-fermion interaction. Applying mean field theory (details are contained in Appendix A and B), leads to:

$$H_{MF} = - \sum_{j=1}^N \left[u(j, j+1) c_j^\dagger c_{j+1} + \frac{iv}{2} c_j^\dagger c_{j+2} \right] + H.C., \quad (5)$$

where c_j^\dagger and c_j are the fermionic creation and annihilation operators satisfying the standard anticommutation relations. Choosing u consistent with PBC, a discrete Fourier transform diagonalizes this Hamiltonian:

$$H_{MF} = \sum_p E(p) c_p^\dagger c_p, \quad E(p) = \tilde{u}(p) + \tilde{u}^*(p) + v \sin p. \quad (6)$$

Here $p \in [-\pi, \pi)$, $E(p)$ is the dispersion relation, and $\tilde{u}(p) = \mathcal{U}e^{ip}$ is the Fourier transform of $u(|(j+1) - j|) = \mathcal{U}$. The Fermi points ($E(p) = 0$) are typically at $p_{R,L} = \pm\pi/2$. However, for $|v| > |\mathcal{U}|$, two additional crossings occur at $p_1 = \sin^{-1}(\frac{\mathcal{U}}{v})$ and $p_2 = \pi - p_1$. The ground state energy density in the thermodynamic limit is:

$$\rho_0 = \frac{1}{2\pi} \int_{p:E(p)<0} dp E(p) = \begin{cases} \frac{2\mathcal{U}}{\pi}, & v \leq \mathcal{U} \\ -\frac{\mathcal{U}^2 + v^2}{v\pi}, & v > \mathcal{U} \end{cases}. \quad (7)$$

A discontinuity in the second derivative of ρ_0 at $|v| = |\mathcal{U}|$ signals a second-order QPT [58].

III. ANALOG BH

The model admits a geometric interpretation in the context of BH physics. To establish this connection, we have assigned the lattice sites of (5) alternately to sublattices A and B , which facilitates the emergence of Dirac-like quasiparticles in the continuum limit with the following 2-D metric (see Appendix B)

$$ds^2 = g(x)dt^2 - 2\sqrt{1 - g(x)} \frac{dt dx}{\mathcal{U}(x)} - \frac{dx^2}{\mathcal{U}^2(x)}, \quad (8)$$

where (t, x) are dimensionless coordinates, $g(x) = 1 - v^2/\mathcal{U}^2(x)$. This is the Gullstrand-Painlevé coordinates of spherically symmetric space-time [78]. Employing the coordinate transformation $(t, x) \rightarrow (\tau, x) \rightarrow (\tau, X)$ via

$$\tau(t, x) = t - \int_{x_0}^x \frac{dz}{\mathcal{U}^2(z)} \frac{v}{g(z)}, \quad dX = \frac{1}{g(x)} \frac{dx}{\mathcal{U}(x)}, \quad (9)$$

brings the metric to the following two generic forms:

$$ds^2 = g(x)d\tau^2 - d\mathcal{X}^2/g(x) = g(x) (d\tau^2 - dX^2), \quad (10)$$

where $d\mathcal{X} = dx/\mathcal{U}(x)$ and $\mathcal{U}(x)$ is arbitrary. To further analyze, we take a specific inhomogeneous form for $\mathcal{U}(x)$:

$$\mathcal{U}(x) = \text{sech}(x/\sigma)/\sqrt{2\sigma}, \quad (11)$$

where σ is a constant. Thus, for $\sigma < \sigma_c \equiv 1/(2v^2)$, the $\tau - \tau$ component of the metric (10) vanishes at two distinct points. This condition signifies the presence of two horizons, defined by $g(x) = 0$ and located at:

$$x_{c\pm} = \pm\sigma \cosh^{-1}\left(\sqrt{\sigma_c/\sigma}\right), \quad \text{if } \sigma < \sigma_c. \quad (12)$$

The emergence of two horizons exhibits a striking resemblance to the Reissner-Nordström (RN) BH solution in 4-D spacetime. The RN metric is given by [79, 80]:

$$d\tilde{s}^2 = f(r) (-dt^2 + dr_*^2) + r^2 d\Omega_2^2, \quad (13)$$

where $f(r) = 1 - 2M/r + Q^2/r^2$, $r_* = \int dr/f(r)$ and, the two horizons are located at $r_{\pm} = M \pm \sqrt{M^2 - Q^2}$.

This is the first key result of this work, which we want to discuss in detail: First, the continuous chiral analog model mimics the 4-D RN BH. At $\sigma = \sigma_c$, the two horizons coincide, similar to the extremal RN BH where $r_{\pm} = 2M$. At this critical value, we find $x_{c\pm} = 0$, mirroring the behavior of the extreme RN solution. In addition, for $\sigma > \sigma_c$, the spacetime remains regular, exhibiting no horizons or naked singularity. Thus, σ effectively plays a role analogous to the charge-to-mass ratio ($Q/M = \sigma/\sigma_c$) in the RN solution. This analogy highlights the crucial role of σ in determining the spacetime structure, particularly the presence or absence of horizons, similar to how M and Q govern the RN BH. This avoidance of naked singularities for $\sigma > \sigma_c$ is consistent with cosmic censorship. In this analog model, σ effectively enforces a form of cosmic censorship, ensuring that when *the charge* represented by σ exceeds a critical value relative to *the mass* (related to σ_c), no naked singularity develops.

Furthermore, despite the global neutrality of the chiral spin chain model (4), effective local charges can arise at each site. This localization stems from the inhomogeneous coupling between sites, resulting in a non-uniform charge distribution across the system. Furthermore, the non-uniformity generates an effective electric field with a $\text{sech}(x)$ profile, exhibiting a

characteristic decrease in strength with distance. This behavior resembles the screening effect in electrostatics, where fields from other charges partially or fully cancel the electric field from a given charge. The non-homogeneous coupling reduces the effective electric field, providing valuable insights into how local interactions influence the field distribution within the spin chain.

To further understand the connection between the analog model and RN BH, we evaluate three geometric quantities for the analog metric (8): the Kretschmann scalar (\mathcal{K}), surface gravity (κ_g), and Komar mass (M_{BH}). \mathcal{K} provides information about the curvature of the space-time and is $\mathcal{K} = 1/(\sigma^4\sigma_c^2)$. Depending on v , $0 < \mathcal{K} < \infty$. The surface gravity and Komar mass are

$$\kappa_g^2 = \frac{1}{8\sigma\sigma_c^2} \left[6 \sinh^2 \left(\frac{x}{\sigma} \right) - \frac{1}{\sigma} \tanh^2 \left(\frac{x}{\sigma} \right) g^2(x) \right], \quad (14)$$

$$M_{BH} = \frac{1}{\sigma_c} \sqrt{\frac{2}{\sigma}} \tan^{-1} \left[\tanh \left(\frac{1}{2} \cosh^{-1} \left[\sqrt{\frac{\sigma_c}{\sigma}} \right] \right) \right]. \quad (15)$$

Later, these quantities will be employed to investigate the nature of the phase transition in the spin-chain and determine whether it exhibits characteristics analogous to a RN BH. In Appendix B, we discuss limits when v or \mathcal{U} vanish or diverge, leading to Carrollian and shockwave limits.

Having established that the chiral spin chain indeed mimics RN BH, the immediate question that needs to be answered is: Can such a system be *observed in the laboratory*? Primarily, where the generation of Hawking radiation often relies on probabilistic processes, a significant challenge arises from the need for active feedback mechanisms. These mechanisms dynamically route quantum systems based on the outcomes of previous interactions, akin to *active switching* in quantum computing [81]. This is particularly demanding in linear wave phenomena scenarios, which are common in analog gravity experiments.

In the rest of this work, we use percolation theory to address this challenge. By carefully designing the initial configuration of the system and employing interactions, we demonstrate the potential to eliminate the need for active feedback. This is achieved by leveraging a static, pre-determined network structure within the analog system. These regions then interact according to the lattice geometry. By carefully choosing this geometry, we can ensure that a percolating cluster emerges, enabling the desired behavior to arise spontaneously.

IV. PERCOLATION MODEL OF A CHIRAL SPIN CHAIN

We now construct a classical bond percolation model [82, 83] that acts as a proxy for the tight-binding model (4). Specifically, like in Refs. [84, 85], we interpret the Hamiltonian (4) in the Fock space as a tight-binding model. A classical percolation model is typically used to study the behavior of connected clusters in a random medium. It involves a lattice where each site or bond is randomly occupied with a probability \mathcal{P} . A large connected cluster emerges at a critical probability \mathcal{P}_c , marking a phase transition.

We define a graph in Fock space to apply this to our system (4). Each node in this graph represents a basis state of the quantum system, specifically a Fock state of fermions with occupation numbers $n_j = 0, 1$. The edges between these nodes correspond to non-zero matrix elements of the Hamiltonian. In other words, an edge connects two nodes if the Hamiltonian has a non-zero transition amplitude between the corresponding Fock states. The Hamiltonian (4) is thus represented on this Fock-space graph by the weights associated with the edges:

$$H_{FS} = \sum_{I \neq K} T_{IK} |I\rangle \langle K| , \quad (16)$$

where H_{FS} in Fock space acts on a graph where nodes represent Fermionic basis states $|I\rangle = |n_1, n_2, \dots, n_N\rangle$. Edges in this graph correspond to off-diagonal matrix elements T_{IK} of H_{FS} , representing hopping between states $|I\rangle$ and $|K\rangle$, i.e., $T_{IK} = \langle I|H_{MF}|K\rangle$, where the NN and NNN fermionic creation and annihilation operator terms inside the bracket correspond to the mean-field Hamiltonian (5). Active edges on the graph represent either NN interactions (\mathcal{U} dominant) or NNN interactions (v dominant). When \mathcal{U} dominates, only edges between NN nodes are active. When v dominates, diagonal edges representing NNN interactions become active. Fig. 1 illustrate these active edges for $N = 3$, with red (left) and blue (right) lines indicating NN and NNN interactions, respectively, and the cube nodes represent Fock states. The percolation cluster is the largest set of connected nodes. A phase transition occurs when the NN and NNN interaction strengths become equal, marking the onset of a *percolation transition* [86, 87].

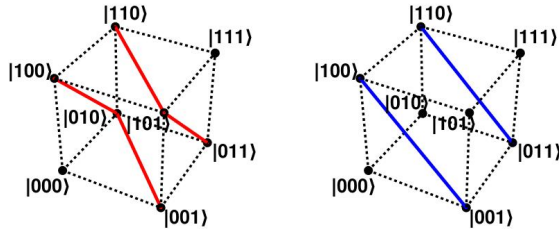


FIG. 1: Fock-space cube illustrating system behavior for dominant NN interactions (red edges in the left figure) and NNN interactions (blue edges in the right figure) in a three-spin system. Nodes represent basis states, and active edges represent allowed transitions.

A. Percolation exponents

To analyze cluster growth, we examine total energy density (ρ_T) and number of clusters (\mathcal{N}) as a function of system size N . To keep the discussion transparent, we consider a deterministic percolation scenario where bond activation is governed by interaction strengths, with no randomness in forming connections. Therefore, we can extract critical exponents by systematically increasing N . To go about this we need to quantify how densely the energy is concentrated within a cluster including the interaction energy (IE). The energy density of an individual cluster is defined as:

$$\text{Energy density} = \frac{\# \text{ of connected bonds}}{\# \text{ of connected states}} \times \text{IE}, \quad (17)$$

where IE is \mathcal{U} for NN and v for NNN interactions. ρ_T is obtained by summing the energy densities of all individual clusters. As shown in Fig. 2, we see two distinct features: When NN interactions dominate, the normalized total energy density of the clusters ρ_T/\mathcal{U} , shown in red (left) and \mathcal{N} shown in red (right) increases linearly with N , indicating a simple connectivity structure. However, when NNN interactions dominate, the normalized total energy density of the clusters ρ_T/v shown in blue (left) and the number of clusters shown in blue (right) exhibit exponential growth, characteristic of a BH-like phase with intricate connectivity. The contrasting growth provides strong evidence for BH phase interpretation.

To further understand the relation between the phase transition of the analog model and RN BH, we analyze the correlation length critical exponent (ν_P) which characterizes the behavior of the correlation length ξ near the percolation transition. Here, ξ corresponds

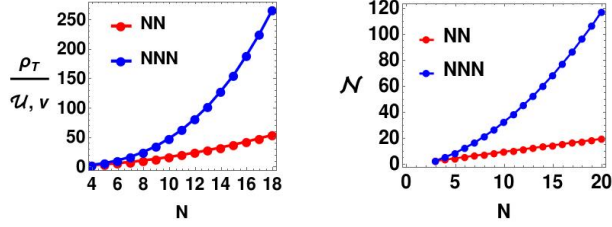


FIG. 2: Normalized cluster energy density (left) and \mathcal{N} (right) vs. system size N . Red (blue) circles: Dominant NN (NNN) interactions.

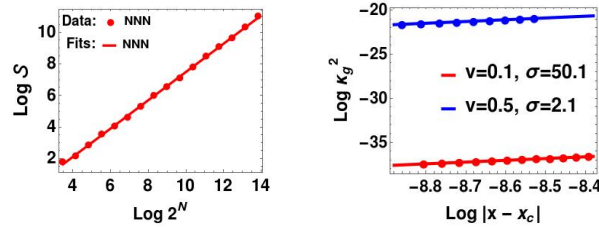


FIG. 3: Plot of $\log \mathcal{S}$ vs $\log 2^N$ (left) and $\log \kappa_g^2$ vs $\log |x - x_c|$ (right). Solid lines are fits to numerical (left) and analytical values using Eq. (14) (right).

to the size of the largest cluster (\mathcal{S}). Near the critical point, ξ follows power law: $\xi \sim |\mathcal{P} - \mathcal{P}_c|^{\nu_P}$ [86, 87]. Since at critical point the system is scale-invariant, implying that ξ must be comparable to the number of Fock states, hence [86, 87]:

$$\xi \sim |\mathcal{P} - \mathcal{P}_c|^{\nu_P} \sim 2^N. \quad (18)$$

By plotting $\log \mathcal{S}$ versus $\log(2^N)$ in Fig. 3 (left), we determine ν_P from the slope of the linear fit. For the dominant NNN interaction, we find $\nu_P = 1.11$. This exponent governs the divergence of the correlation length at the critical point and will be used to determine critical exponent corresponding to the total energy (E_T) of the system. The total energy, E_T , is

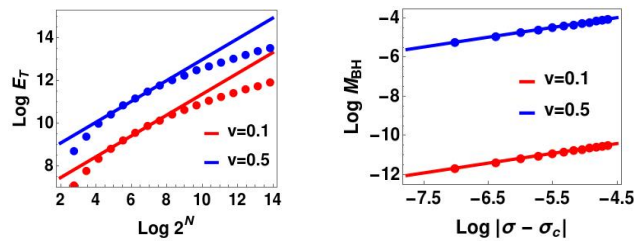


FIG. 4: Plot of $\log E_T$ vs $\log 2^N$ (left) and $\log M_{BH}$ vs $\log |\sigma - \sigma_c|$ (right). Solid lines are the fits to the numerical (Left) and analytical values using Eq. (15) (Right).

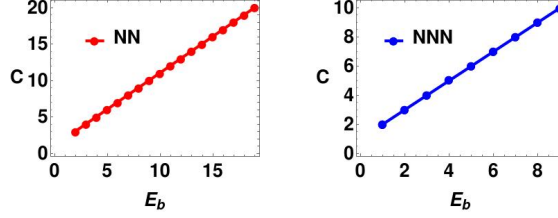


FIG. 5: Plot of circumference C of the smallest cluster and the energy of connected bonds E_b for dominating NN (left) and NNN (right) phase.

calculated by multiplying ρ_T with the total number of states. Since, E_T changes due to IE, like ξ , E_T also diverges at the critical point allowing us to write $E_T \sim |\mathcal{P} - \mathcal{P}_c|^\beta \sim (2^N)^{\frac{\beta}{\nu_P}}$. The left Fig. 4 is the plot of $\log E_T$ versus $\log(2^N)$ for two values of ν , and \mathcal{U} given by (11). From the slope of the linear fit around the transition, we obtain β/ν_P yielding $\beta = 0.53$ for the dominant NNN interaction case.

Fig. 5 shows the number of connected bonds E_b , and the number of states C in the smallest cluster. The equal slopes of the plotted lines for both the NN- and NNN-dominated phases suggest that the hoop conjecture [88–91], should be satisfied, requiring $\mathcal{U} \geq 1$ in the NN phase and $\nu \geq 1$ in the NNN phase. However, our analysis reveals that $\nu \geq \mathcal{U}$, a condition necessary for BH formation, is *not* satisfied. This indicates that the hoop conjecture, within our percolation model, does not impose stringent conditions favoring one phase over the other for BH formation. While geometrically satisfying the hoop conjecture within the percolation model appears to be a *necessary* condition for the emergence of a BH-like object, our results suggest it is not *sufficient* [92].

Percolation Model (NNN phase)		Gravitational Collapse (BH phase)	
Quantity	Critical Exponent	Quantity	Critical Exponent
Correlation length (ξ): $\xi \sim \mathcal{P} - \mathcal{P}_c ^{\nu_P}$	$\nu_P = 1.11$	Surface gravity (κ_g): $\kappa_g \propto (x - x_c)^\gamma$	$\gamma = 1.00$
Total energy (E_T): $E_T \sim \mathcal{P} - \mathcal{P}_c ^\beta$	$\beta = 0.53$	Black hole mass (M_{BH}): $M_{BH} \propto (\sigma - \sigma_c)^{\gamma_M}$	$\gamma_M = 0.5$

TABLE I: Comparison of critical exponents between the percolation model and gravitational collapse.

A key finding of this work is the exceptional agreement between the numerically calculated

scaling exponents for the lattice model (with $N \leq 20$) and the corresponding analytical results for the continuum limit. This agreement is clearly demonstrated by the comparison of surface gravity (Fig. 3, right) and Komar mass (Fig. 4, right), and is further detailed in Table I. As N increases, this comparison is expected to become exact.

V. CONCLUSIONS

Our results offer significant insights into the analog model and its connection to BH physics. The exceptional agreement between numerical results for finite lattice sizes and analytical predictions for the continuum model demonstrates the robustness of this analog system in capturing key features of gravitational collapse. This is consistent with established mappings between quantum spin chains and classical percolation models [82–84], where a phase transition at the percolation threshold mirrors critical phenomena in the spin chain. This transition reflects a change in lattice connectivity analogous to the behavior observed in quantum systems at criticality.

This percolation framework describes gravitational collapse and BH formation. The emergence of an event horizon is analogous to reaching the percolation threshold, with distinct regions inside and outside the horizon reflecting the transition between physical phases. The close alignment of scaling exponents derived from the analog model with those of surface gravity and Komar mass in the BH context further validate this framework. Crucially, the exponential cluster growth observed in analogous to matter aggregation during stellar collapse.

Our results also shed light on the hoop conjecture [88–91] and opens a new avenue for exploring BH-like phenomena in complex systems by highlighting the importance of additional criteria beyond the geometric hoop conjecture. Specifically, the exponential growth of clusters and energy is a key indicator of BH formation in this analog system, potentially acting as a proxy for the *hoop* itself. Furthermore, the observed formation of a horizon-like structure, coupled with the absence of naked singularities for $\sigma > \sigma_c$, provides further support for cosmic censorship within this analog framework.

This analysis provides a step towards understanding matter/energy organization within a BH event horizon, a region inaccessible to direct observation in astrophysical BHs. By simulating BHs in the lab via this analog system, we can begin to probe these questions

without needing a full theory of BH singularities. This work focuses on the classical aspects of the percolation and gravity sides. Future quantum extensions, incorporating superposition and entanglement, will allow us to explore Hawking radiation and BH information paradox, especially at the critical value $\sigma = \sigma_c$ when the horizons degenerate and surface gravity vanishes. Specifically, the entanglement entropy arising from quantum correlations between sites within and outside forming clusters may correspond to BH entropy [75], offering insights into the information encoded within the horizon. These quantum extensions are under investigation.

ACKNOWLEDGMENTS

The authors thank G. Baskaran, Indranil Chakraborty, K. Hari, P. George Christopher, Susobhan Mandal, Tausif Parvez, Tapobrata Sarkar, and Semin Xavier for discussions and comments on the earlier draft. The work is supported by SERB-CRG (RD/0122-SERB000-044).

Appendix A: Jordan-Wigner and Fourier transformations

Our starting point is a system of N spin-1/2 particles arranged in a one-dimensional periodic chain with inhomogeneous nearest-neighbor (NN) and chiral interactions. The Hamiltonian governing the system is given by

$$\tilde{H} = - \sum_{j,k=1}^N \frac{U(j,k)}{2} (\sigma_j^x \sigma_k^x + \sigma_j^y \sigma_k^y) + \sum_{j=1}^{N-2} \frac{vV(j,j+2)}{4} (\vec{\sigma}_j \cdot (\vec{\sigma}_{j+1} \times \vec{\sigma}_{j+2})) , \quad (\text{A1})$$

where v is a constant, $U(j,k)$ and $V(j,j+2)$ are site-dependent coupling constants introducing spatial inhomogeneity into the system. Here, the operators $\sigma_j^{x,y,z}$ represent the Pauli matrices at the j -th site, and $\vec{\sigma}_j = (\sigma_j^x, \sigma_j^y, \sigma_j^z)$ denotes the Pauli matrix vector of the j -th spin. The first term of the Hamiltonian describes an inhomogeneous spin-1/2 XX interaction between sites j and k , while the second term represents a three-spin chiral interaction involving consecutive spins at sites j , $j+1$, and $j+2$. The physical properties of the system are determined by the relative strength of the two coupling constants $U(j,k)$ and $V(j,j+2)$. To simplify the analysis, we can rescale the Hamiltonian by the coupling constant $V(j,j+2)$

which yields

$$\tilde{H} = \sum_{j,k=1}^N V(j, j+2) H(j, k), \quad \text{with} \quad H(j, k) = -\frac{u(j, k)}{2} (\sigma_j^x \sigma_k^x + \sigma_j^y \sigma_k^y) + \frac{v}{4} (\vec{\sigma}_j \cdot (\vec{\sigma}_{j+1} \times \vec{\sigma}_{j+2})), \quad (\text{A2})$$

where $u(j, k) = \frac{U(j, k)}{V(j, j+2)}$. Since we have a one-dimensional system, without loss of generality, we can restrict the coupling constants $u(j, k) \equiv u(|j - k|)$, and $V(j, j + 2) \equiv V(|(j + 2) - j|)$, to depend only on the distance between the sites so that the system remains translationally invariant. Later in this section while performing the Fourier transformation, we will show that $V(j, j + 2)$ only modifies the overall energy scale of the system. In the continuum limit, the system is described by a massless, minimally coupled Dirac field in a (1+1)-dimensional curved spacetime. Since the curved spacetime is locally conformal to the Minkowski space, the dynamics of the Dirac field remain unchanged up to a simple rescaling. Thus, the coupling $V(j, j + 2)$ merely acts as a conformal factor to the spatial metric in the continuum limit. The key properties of the Hamiltonian \tilde{H} remain unchanged if we remove this conformal factor. Hence, we can work with the rescaled Hamiltonian of the form

$$H = - \sum_{j,k=1}^N \frac{u(|j - k|)}{2} (\sigma_j^x \sigma_k^x + \sigma_j^y \sigma_k^y) + \sum_{j=1}^{N-2} \frac{v}{4} (\vec{\sigma}_j \cdot (\vec{\sigma}_{j+1} \times \vec{\sigma}_{j+2})), \quad (\text{A3})$$

which preserves the essential physics of the system while eliminating unnecessary rescaling. Here, j, k are now identified as NN sites and the coupling $u(|j - k|)$ makes the system inhomogeneous and becomes the source of curvature in the continuum limit. In order to discuss the mean-field theory and analytic results, we apply a Jordan-Wigner transformation which maps spin-1/2 Pauli operators to spinless fermions defined as

$$\sigma_j^+ = \exp\left(-i\pi \sum_{l=1}^{j-1} c_l^\dagger c_l\right) c_j^\dagger, \quad \sigma_j^- = \exp\left(i\pi \sum_{l=1}^{j-1} c_l^\dagger c_l\right) c_j, \quad \sigma_j^z = 1 - 2c_j^\dagger c_j, \quad (\text{A4})$$

where $\sigma_j^\pm = (\sigma_j^x \pm \sigma_j^y)/2$ and c_j are fermionic operator satisfying anti-commutation relations $\{c_j, c_k^\dagger\} = \delta_{jk}$ and $\{c_j, c_k\} = \{c_j^\dagger, c_k^\dagger\} = 0$. The mapping of the chirality operator, $\chi_j = \vec{\sigma}_j \cdot (\vec{\sigma}_{j+1} \times \vec{\sigma}_{j+2})$, to the Fermionic Hamiltonian has been extensively discussed in [66, 67]. However, since the first term in the original Hamiltonian is non-trivial, we focus here on its explicit mapping to the fermionic representation. For completeness, we derive the mapping for both the original Hamiltonian and the rescaled Hamiltonian. The first terms of Eq. (A2)

and the rescaled Hamiltonian in Eq. (A3) are given by:

$$\tilde{H}_{XX} = - \sum_{j,k=1}^N V(|(j+2)-j|)u(|j-k|) \left(c_j^\dagger c_k + c_k^\dagger c_j \right) , \quad H_{XX} = - \sum_{j,k=1}^N u(|j-k|) \left(c_j^\dagger c_k + c_k^\dagger c_j \right) . \quad (\text{A5})$$

Although the model is inhomogeneous, the above Hamiltonians in Eq. (A5) remain translationally invariant because $u(|j-k|)$ depend solely on the distance between sites. Consequently, it can be exactly diagonalized using the discrete Fourier transformation

$$c_j = \frac{1}{\sqrt{N}} \sum_{p \in [-\pi, \pi)} e^{ipj} c_p , \quad c_j^\dagger = \frac{1}{\sqrt{N}} \sum_{p \in [-\pi, \pi)} e^{-ipj} c_p^\dagger , \quad (\text{A6})$$

where the quasi-momentum p takes the values $p = \frac{2\pi\lambda}{N}$ for $\lambda \in \mathbb{Z}$ so that the Hamiltonian (A5) takes the following form:

$$\begin{aligned} \tilde{H}_{XX} &= -\frac{1}{N} \sum_{p,p'} \sum_{j,k=1}^N V(|(j+2)-j|)u(|j-k|) e^{i(p'j-pk)} c_p^\dagger c_{p'} + H.C. , \\ H_{XX} &= -\frac{1}{N} \sum_{p,p'} \sum_{j,k=1}^N u(|j-k|) e^{i(p'j-pk)} c_p^\dagger c_{p'} + H.C. . \end{aligned} \quad (\text{A7})$$

Rewriting it, we have:

$$\tilde{H}_{XX} = - \sum_p \mathcal{V} \tilde{u}(p) c_p^\dagger c_p + H.C. , \quad H_{XX} = - \sum_p \tilde{u}(p) c_p^\dagger c_p + H.C. , \quad (\text{A8})$$

where $\mathcal{V} = V(|(j+2)-j|)$, and $\tilde{u}(p) = \sum_l u(l) e^{ipl}$ with $l = j-k$. Now if j and k are the NN indices, then $\tilde{u}(p) = \mathcal{U} e^{ip}$ with $\mathcal{U} = u(|(j+1)-j|)$. Using the results of Ref. [66, 67, 74], the complete Hamiltonians (A2) and (A3) in diagonalized form in the mean field approximation [67] is written as

$$\tilde{H}_{MF} = \sum_p \tilde{E}(p) c_p^\dagger c_p , \quad H_{MF} = \sum_p E(p) c_p^\dagger c_p , \quad (\text{A9})$$

with $\tilde{E}(p) = \mathcal{V} E(p)$, and $E(p) = -2\mathcal{U} \cos(p) + v \sin(2p)$.

Appendix B: The continuum limit and emergent black hole background

To investigate the geometric aspects of the model and its connection to general relativity, it is essential to derive the corresponding continuum limit. This is accomplished by

performing a Taylor expansion of the mean-field Hamiltonian around the Fermi points, in the vicinity of which the Dirac cone is located. Near the Fermi points, the linear part of the dispersion relation dominates, while the non-linear part becomes negligible at high momenta. As shown in Refs. [66, 67, 74], we assign lattice sites alternately to sublattices A and B , forming a two-site unit cell, to facilitate the continuum limit analysis. This sublattice arrangement allows Dirac-like quasiparticles to emerge in the continuum limit, exhibiting a linear dispersion relation characteristic of relativistic dynamics.

The complete mean-field Hamiltonian in terms of Jordan-Wigner fermions of sub-lattices A and B , and using Eq. (A5) is $\tilde{H}_{MF} = \mathcal{V}H_{MF}$, where:

$$H_{MF} = - \sum_{j=1}^{N_c} \left(\mathcal{U} \left(a_j^\dagger b_j + a_j b_{j-1}^\dagger \right) + \frac{iv}{2} \left(a_j^\dagger a_{j+1} + b_j^\dagger b_{j+1} \right) \right) + H.C. , \quad (\text{B1})$$

the fermionic operators satisfy anti-commutation relations $\{a_j, a_k^\dagger\} = \{b_j, b_k^\dagger\} = \delta_{jk}$ and all other anti-commutators vanishes, and $N_c = N/2$ is the number of unit cells. The Fourier transformation of the unit cell operators a_j and b_j are defined by

$$a_j = \frac{1}{\sqrt{N_c}} \sum_{p \in [-\pi, \pi]} e^{ipa_c j} a_p , \quad b_j = \frac{1}{\sqrt{N_c}} \sum_{p \in [-\pi, \pi]} e^{ipa_c j} b_p , \quad (\text{B2})$$

where, $a_c = 2a$ is the unit cell spacing for a given lattice spacing a . Applying this we can rewrite the mean-field Hamiltonian as

$$\tilde{H}_{MF} = \sum_p (F(p) a_p^\dagger b_p + F^*(p) b_p^\dagger a_p) + \sum_p G(p) (a_p^\dagger a_p + b_p^\dagger b_p) , \quad (\text{B3})$$

where $F(p) = -\mathcal{U}(1 + e^{-ia_c p})\mathcal{V}$ and $G(p) = v\mathcal{V} \sin(a_c p)$. In terms of two-component spinor $\chi_p = (a_p, b_p)^T$ and the single particle Hamiltonian $h(p)$, the complete mean-field Hamiltonian

$$\tilde{H}_{MF} = \sum_p \chi_p^\dagger h(p) \chi_p , \quad h(p) = \begin{pmatrix} G(p) & F(p) \\ F^*(p) & G(p) \end{pmatrix} , \quad (\text{B4})$$

with the dispersion relation taking the form

$$\tilde{E}(p) = \pm \mathcal{V} \left(\mathcal{U} \sqrt{2 + 2 \cos(a_c p)} + v \sin(a_c p) \right) .$$

The continuum limit is derived by performing a Taylor expansion of the single-particle Hamiltonian $h(p)$ around the Fermi points. These Fermi points are defined as the momenta where the dispersion relation $\tilde{E}(p) = 0$ holds, as discussed in Refs. [66, 67]. Specifically, the

Fermi points are located at $p_0 = \frac{\pi}{a_c}$, and $p_1 = \frac{1}{a_c} \arccos(1 - \frac{2\mathcal{U}^2}{v^2})$, with the second Fermi point p_1 existing only when the condition $|v| > |\mathcal{U}|$ is satisfied. To obtain the continuum theory, we perform a Taylor expansion of the functions $F(p)$ and $G(p)$ around the Fermi point p_0 , retaining terms up to first order in momentum, giving

$$h(p_0 + p) = a_c \mathcal{U} \mathcal{V} \sigma^y p - a_c v \mathcal{V} p \mathbb{1} + \mathcal{O}(p^2) \equiv e_a^l \alpha^a p_l, \quad (\text{B5})$$

where the coefficients are defined as $e_0^x = -a_c v \mathcal{V}$, $e_1^x = a_c \mathcal{U} \mathcal{V}$; and the Dirac matrices $\alpha^0 = \mathbb{1}$, $\alpha^1 = \sigma^y$. The continuum limit of the model is obtained by letting the unit cell spacing $a_c \rightarrow 0$ and the thermodynamic limit $N_c \rightarrow \infty$ in such a way that $N_c a_c$ is constant. Then we renormalize the couplings $a_c \mathcal{U} \rightarrow \mathcal{U}$ and $a_c v \rightarrow v$, and defining the continuum limit coordinate $x = j a_c$, the continuum limit Hamiltonian after an inverse Fourier transformation to real space takes the form

$$\tilde{H} = \int_{\mathbb{R}} dx \chi^\dagger(x) \left(-i e_a^l \alpha^a \overset{\leftrightarrow}{\partial}_l \right) \chi(x), \quad (\text{B6})$$

where we have defined the two-component spinor field $\chi(x) = (a(x), b(x))$, the inhomogeneous couplings \mathcal{U} and \mathcal{V} become space-dependent $\mathcal{U} \equiv \mathcal{U}(x)$ and $\mathcal{V} \equiv \mathcal{V}(x)$, $A \overset{\leftrightarrow}{\partial}_\mu B = \frac{1}{2} (A \partial_\mu B - (\partial_\mu A) B)$, and the Dirac matrices $\alpha^a = (\mathbb{1}, \sigma^y)$ and $\beta = \sigma^z$. The corresponding action for the Hamiltonian (B6) is given by

$$S = \int_{\mathbb{M}} d^{1+1}x \chi^\dagger(x) \left(i \overset{\leftrightarrow}{\partial}_t + i e_a^l \alpha^a \overset{\leftrightarrow}{\partial}_l \right) \chi(x) = \int_{\mathbb{M}} d^{1+1}x \bar{\chi}(x) i e_a^\mu \gamma^a \overset{\leftrightarrow}{\partial}_\mu \chi(x), \quad (\text{B7})$$

with \mathbb{M} being the Minkowski space, $\gamma^0 = \beta = \sigma^z$, and $\gamma^l = \beta \alpha^l$ implies $\gamma^1 = -i \sigma^x$ and $\bar{\chi} = \chi^\dagger \sigma^z$. The gamma matrices obey the anti-commutation relation $\{\gamma^a, \gamma^b\} = \eta^{ab}$ with $\eta^{ab} = \text{diag}(1, -1)$. This action closely resembles that of a Dirac field in a (1+1)-dimensional curved spacetime [28, 93, 94], but with two notable distinctions. First, the integration measure lacks the factor of $|e|$, effectively reducing it to the flat spacetime volume element. Second, the fields satisfy flat spacetime anti-commutation relations, given by $\{\chi_\alpha(x), \chi_\beta(y)\} = \delta_{\alpha\beta} \delta(x - y)$ [74]. To interpret this theory within the framework of curved spacetime, we introduce a spinor field $\psi = \chi / \sqrt{|e|}$ which obey the anti-commutation relation $\{\psi_\alpha(x), \psi_\beta(y)\} = \frac{\delta_{\alpha\beta} \delta(x-y)}{|e|}$ and propagate on a spacetime with tetrad e_a^μ with $|e|$ being the determinant of the tetrad e_a^μ , which correspond to the metric $g^{\mu\nu} = e_a^\mu e_b^\nu \eta^{ab}$, explicitly given by

$$e_a^\mu = \begin{pmatrix} 1 & -v \mathcal{V}(x) \\ 0 & \mathcal{U}(x) \mathcal{V}(x) \end{pmatrix}, \quad g^{\mu\nu} = \begin{pmatrix} 1 & -v \mathcal{V}(x) \\ -v \mathcal{V}(x) & \mathcal{V}^2(x) (v^2 - \mathcal{U}^2(x)) \end{pmatrix}. \quad (\text{B8})$$

When re-expressed in terms of the field ψ , the action of Eq. (B7) exactly corresponds to the Dirac action for a spinor field on a spacetime with the following line-element:

$$ds^2 = g(x)dt^2 - 2\sqrt{1-g(x)}\frac{dt dx}{\mathcal{U}(x)} - \frac{dx^2}{\mathcal{U}^2(x)}, \quad (\text{B9})$$

where $g(x) = 1 - v^2/\mathcal{U}^2(x)$ and we have redefined the spatial coordinate $x \rightarrow x \mathcal{V}(x)$ since $\mathcal{V}(x)$ only acts as a conformal factor to the spatial part of the metric. This is the Gullstrand-Painlevé coordinates of spherically symmetric space-time [78]. Employing the coordinate transformation $(t, x) \rightarrow (\tau, x) \rightarrow (\tau, X)$ via

$$\tau(t, x) = t - \int_{x_0}^x \frac{dz}{\mathcal{U}^2(z)} \frac{v}{g(z)}, \quad dX = \frac{1}{g(x)} \frac{dx}{\mathcal{U}(x)}, \quad (\text{B10})$$

brings the metric to the following two generic forms:

$$ds^2 = g(x)d\tau^2 - d\mathcal{X}^2/g(x) = g(x) (d\tau^2 - dX^2), \quad (\text{B11})$$

where $d\mathcal{X} = dx/\mathcal{U}(x)$ and $\mathcal{U}(x)$ is still arbitrary.

It is important to note that the usual scaling dimension of a Dirac field $\Delta = 1/2$ in a 1+1-dimensional curved spacetime can be recovered by considering the above redefinition of the spinor field $\psi = \chi/\sqrt{|e|}$. Further, it is easy to verify the scale invariance of the Hamiltonian (B6). Under a scaling transformation $x \rightarrow \Lambda x$, the field and couplings scale as

$$\chi(x) \rightarrow \Lambda^{-\Delta} \chi(\Lambda x), \quad v \rightarrow \Lambda^{\beta_v} v, \quad \mathcal{U}(x) \rightarrow \Lambda^{\beta_u} \mathcal{U}(\Lambda x), \quad \mathcal{V}(x) \rightarrow \Lambda^{\beta_v} \mathcal{V}(\Lambda x), \quad (\text{B12})$$

Δ being the scaling dimension of the field, β_v is the scaling dimension of the coupling v , and β_u and β_v are the scaling dimension of the space-dependent couplings $\mathcal{U}(x)$ and $\mathcal{V}(x)$ respectively, then the Hamiltonian

$$\tilde{H} \rightarrow \Lambda^{1-2\Delta-1} \int_{\mathbb{R}} dx \chi^\dagger(\Lambda x) (-ie_0^x \alpha^0 \Lambda^{\beta_v+\beta_v+1} - ie_1^x \alpha^1 \Lambda^{\beta_u+\beta_v+1}) \overleftrightarrow{\partial}_x \chi(\Lambda x). \quad (\text{B13})$$

For the Hamiltonian to be scale-invariant: $-2\Delta + \beta_v + \beta_v + 1 = 0$ and $-2\Delta + \beta_u + \beta_v + 1 = 0$, which gives the scaling dimension of the field $\Delta = (\beta_u + \beta_v + 1)/2$ imposing the constraint $\beta_u = \beta_v$.

1. Interesting limits of the BH metric

Let us now explore the interesting limits of the metric Eq. (B9).

a. Carrollian limit

Setting $v = 0$ in the above metric, the dispersion relation near the Fermi point p_0 becomes $E(p + p_0) = \pm \mathcal{U}(x) \sqrt{(\pi - a_c p)^2}$. In the limit of $\mathcal{U}(x) \rightarrow 0$, the momentum-space dispersion relation flattens completely, corresponding to the Carrollian limit ($c \rightarrow 0$) [95, 96]. This limit is associated with the collapse of the position-space light cone, where c represents the speed of light. When $v = 0$, the Hamiltonian (Eq. B6) simplifies to:

$$H = \int_{\mathbb{R}} dx \chi^\dagger(x) \left(-i \mathcal{U}(x) \sigma^y \overleftrightarrow{\partial}_x \right) \chi(x). \quad (\text{B14})$$

Up to a negative sign and the presence of $\mathcal{U}(x)$, this Hamiltonian is mathematically equivalent to a Carrollian Hamiltonian with *upper gamma matrices* [95, 96]. This highlights the direct connection to the Carrollian framework. Note that x is an arbitrary spatial coordinate. Choosing a different spatial coordinate, such as y , would not fundamentally change the physics; the form of the Pauli matrix (σ in this case) would simply reflect the chosen coordinate system.

b. Conformally diverging geometry

In the limit of $\mathcal{U}(x) \rightarrow 0$ but with finite v , the metric (B9) reduces to

$$ds^2 \approx -\frac{1}{\mathcal{U}^2(x)} (v^2 dt^2 + 2v dt dx + dx^2) = -\frac{1}{\mathcal{U}^2(x)} (d\tilde{t} + dx)^2, \quad (\text{B15})$$

with $\tilde{t} = vt$, and $-\frac{1}{\mathcal{U}^2(x)}$ serves as the conformal factor which diverges, making the spacetime structure poorly behaved.

c. Shock wave geometry

If we choose $\mathcal{U}(x)$ to be $\ln|x - x_0|$, $\exp\left(\frac{1}{x-x_0}\right)$, or similar forms, then $\mathcal{U}(x) \rightarrow \infty$ as $x \rightarrow x_0$. In such cases, the metric becomes purely timelike at $x = x_0$ for trajectories where $dt \neq 0$. This situation can be associated with a gravitational shock wave, as these functions introduce discontinuities in the metric similar to those produced by gravitational shock waves generated by massless [97, 98], or massive particles [99]. However, unlike typical gravitational shock waves, which are associated with null hypersurfaces, the shock wave in this case is associated with timelike hypersurfaces. This distinction is crucial: timelike

hypersurfaces permit two-way communication across the boundary, while null hypersurfaces are causally one-directional, corresponding to signals propagating at the speed of light.

The discontinuity in the metric could also represent phenomena such as a domain wall or an interface between two regions of spacetime with different physical properties. It might also correspond to a sharp concentration of matter or energy localized on a timelike hypersurface, such as a thin shell.

However, in the main text we considered $\mathcal{U}(x)$ to be free of such discontinuities, ensuring a well-behaved metric throughout the region of interest. In particular, $\mathcal{U}(x) \sim \text{sech}(x)$ is particularly suitable due to its smoothness and exponential decay, avoiding singularities and providing a consistent and physically meaningful framework.

Appendix C: BH critical exponents

Near the threshold of BH formation, a striking phenomenon known as critical behavior emerges [68]. Much like in phase transitions, the properties of a forming BH do not evolve smoothly but instead follow power-law scaling. As an initial condition parameter (η) — such as the strength of an incoming matter wave — approaches a critical value (η_*), the resulting BH's mass ($M_{BH} \propto (\eta - \eta_*)^{\gamma_M}$ where γ_M is the critical exponent) follows a power-law dependence, characterized by a critical exponent [100, 101]. Remarkably, these exponents, along with others governing different physical quantities, often exhibit *universality*, meaning they remain the same regardless of the specific nature of the collapsing matter. This universality suggests a deeper underlying structure within Einstein's equations and points to intriguing connections between BH formation and broader studies of critical phenomena, potentially shedding light on the quantum aspects of gravity [84, 102, 103].

Broadly there are two regimes in this scenarios: First, the supercritical regime, where black holes of arbitrarily small mass can form. In this regime, the BH mass M_{BH} scales as $M_{BH} \propto (\eta - \eta_*)^{\gamma_M}$ where $|\eta - \eta_*|^{\gamma_M}$ has the dimensions of length. Second, the subcritical regime, where the maximum scalar curvature R_{max} before the field disperses scales as $R_{max} \propto (\eta - \eta_*)^{-2\gamma}$ [100, 101]. If our analog model truly mimics black hole formation, it should reproduce these critical exponents. Therefore, it is of interest to explore the relationship between the critical exponents γ_M and γ within the context of the analog metric (10), specifically in $D = 2$. While the relation $\gamma_M = (D - 3)\gamma$ has been established for higher

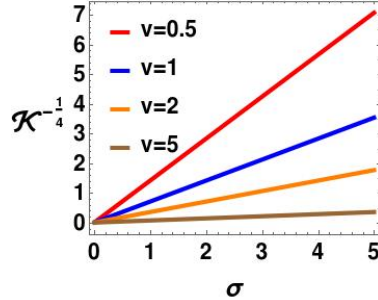


FIG. 6: Inverse fourth root of the Kretschmann scalar, $\mathcal{K}^{-1/4} = \sigma\sqrt{\sigma_c}$ as a function of σ for four different values of $v = 0.5, 1, 2,$ and 5 .

dimensions ($D \geq 4$) [103], we investigate whether a similar or modified scaling relation applies in $D = 2$.

1. Kretschmann scalar and surface gravity

In our study, we focus on the Kretschmann scalar (\mathcal{K}), a quadratic scalar invariant having dimensions $[L]^{-4}$. Defined as $\mathcal{K} = R_{\mu\alpha\beta\rho}R^{\mu\alpha\beta\rho}$, the Kretschmann scalar, unlike the Ricci scalar, remains non-zero in vacuum regions, providing valuable information where the Ricci scalar is trivial. For the metric (10), we find the Kretschmann scalar, $\mathcal{K} = 1/(\sigma^4\sigma_c^2)$ which is independent of x .

Since \mathcal{K} is constant in this scenario, a standard scaling analysis is not possible, and thus \mathcal{K} cannot directly yield critical exponents. However, as shown in Fig. 6, our numerical results confirm a linear relationship between $\mathcal{K}^{-1/4}$ and σ for different values of v . This linearity suggests a connection to the critical behavior, as $\sigma - \sigma_c$ quantifies the proximity to the critical point. The absence of scaling in \mathcal{K} indicates that it is likely not the optimal quantity for directly determining the correlation length exponent.

This leads us to surface gravity, which is defined as

$$\kappa_g^2 = -\frac{1}{2}(\nabla_\mu K_\nu)(\nabla^\mu K^\nu), \quad (\text{C1})$$

K^μ is the Killing vector associated with the Killing horizon Σ , and n^μ is the unit normal vector to the horizon surface. According to the zeroth law of BH mechanics, the surface gravity of a stationary BH is constant over the event horizon and independent of the observer. To confirm the scaling exponent of the surface gravity, we evaluate it at the horizon. For

the metric (10), the components of the Killing vector are: $K^\mu = (1, 0)$ and $K_\mu = (g(x), 0)$, while the components of the the normal vector are:

$$n^\mu = \left(\sqrt{g(x)}, 0 \right) , \quad n_\mu = \left(\frac{1}{\sqrt{g(x)}}, 0 \right) . \quad (\text{C2})$$

These vectors are normalized such that $K^\mu K_\mu = n^\mu n_\mu = 1$. At the event horizon ($v = \mathcal{U}$), we can verify that $K^\mu K_\mu = 0$, $n^\mu n_\mu = 0$, and $K^\mu n_\mu = 0$. Thus, the Killing vector is not only null but also orthogonal to the horizon itself, confirming that the event horizon is a Killing horizon. The surface gravity is then given by:

$$\kappa_g^2 = \frac{1}{8\sigma\sigma_c^2} \left[6 \sinh^2 \left(\frac{x}{\sigma} \right) - \frac{1}{\sigma} \tanh^2 \left(\frac{x}{\sigma} \right) g^2(x) \right] . \quad (\text{C3})$$

Using this expression of κ_g^2 , we analyze its critical exponent and compare it with the correlation length exponent ν_P computed in subsection IV A. The scaling behavior is numerically validated and presented in Fig. 3 (right), where we plot $\log \kappa_g^2$ as a function of $\log |x - x_c|$. Here, x is chosen close to x_c for specific values of σ and v , corresponding to spacetimes near the threshold of BH formation (subcritical collapse). In Fig. 3 (right), the filled circles are the analytical values obtained through Eq. (14), while the solid lines are the numerical fits confirming the linear scaling behavior. For the red curve, corresponding to parameter values $v = 0.1$ and $\sigma = 50.1$, the linear fit follows the relation $\kappa_g^2 = (x - x_c)^{2.00}$. Similarly, for the blue curve, with $v = 0.5$ and $\sigma = 2.1$, the linear fit also adheres to $\kappa_g^2 = (x - x_c)^{2.00}$, up to an unimportant constant in each case. These results demonstrate that the critical exponent associated with the gravitational field strength, represented by the surface gravity, is $\gamma = 1.00$.

Interestingly, we observe that the correlation length exponent $\nu_P = 1.11$ for the NNN dominating phase, referred to as the *black hole phase* in our percolation model, closely matches the exponent $\gamma = 1.00$ associated with the gravitational field strength. This agreement suggests that the formation of clusters in the percolation model mimics the structure and dynamics of the gravitational collapse leading to BH formation.

2. Komar mass

To make the connections between the percolation model and gravitational collapse more concrete, we now turn to the Komar mass, which represents the total mass (or energy)

contained within the spacetime, as seen from infinity. The Komar mass M_K for $(1 + 1)$ -D space-time in terms of Killing vector K^ν is given by [104],

$$M_K = \int_S dx \sqrt{|g|} n_\mu R^{\mu\nu} K_\nu , \quad (\text{C4})$$

where S is a 1-dimensional constant time slice, g is the determinant of the 1-dimensional metric of Eq. (10), n^μ is a unit vector orthogonal to S , and $R^{\mu\nu}$ is the Ricci tensor. Using the Killing equation: $\nabla^\mu K^\nu + \nabla^\nu K^\mu = 0$ and the Killing vector lemma: $\nabla_\nu \nabla_\mu K^\mu = R_{\mu\nu} K^\nu$, the Komar mass can be expressed as

$$M_K = \int_S dx \sqrt{|g|} n_\mu \nabla_\nu (-\nabla^\nu K^\mu) , \quad (\text{C5})$$

with the forms of K^μ and n_μ given in Eq. (C2). The boundary of S has two contributions, one from an inner boundary at the horizon which is the mass of the BH, denoted by M_{BH} and the second from an outer boundary at infinity which is the contribution of matter outside the event horizon to the total mass, denoted by M_∞ . With these inputs, we can write the Komar mass: $M_K = M_{BH} + M_\infty$, where

$$M_{BH} = \frac{1}{\sigma_c} \sqrt{\frac{2}{\sigma}} \tan^{-1} \left[\tanh \left(\frac{1}{2} \cosh^{-1} \left[\sqrt{\frac{\sigma_c}{\sigma}} \right] \right) \right] , \quad (\text{C6})$$

$$M_\infty = -\frac{1}{\sqrt{2}\sigma_c \sigma^{3/2}} \int_{S \rightarrow \infty} dx \operatorname{sech} \left(\frac{x}{\sigma} \right) . \quad (\text{C7})$$

We analyze the numerical scaling of the BH mass (M_{BH}) with σ , which determines proximity to the critical point (σ_c). Since $\sigma - \sigma_c$ quantifies the distance from this threshold, this scaling reveals insights into the critical behavior of the system and gravitational collapse dynamics. Figure 4 (right) shows analytical values (circles) and numerical fits (lines) validating the scaling. For $v = 0.1$ (red) and $v = 0.5$ (blue), the fits follow $M_{BH} \propto (\sigma - \sigma_c)^{0.5}$, confirming a critical exponent $\gamma_M \approx 0.5$. This is in close agreement with $\gamma_M = 0.53$ found in 2-D dilaton gravity [105].

Two key observations emerge from our analysis. First, the critical exponent $\beta = 0.53$ for total energy in the NNN-dominant phase (see subsection IV A) aligns with γ_M , suggesting that clustering dynamics in the percolation model closely resemble the structural and dynamical features of gravitational collapse leading to BH formation, highlighting the relevance of percolation theory in capturing key aspects of gravitational field scaling. Table I compares these exponents. Second, the relationship between the critical exponents γ_M and γ for our

BH metric Eq. (10) in $D = 2$ spacetime dimensions deviates from the conventional scaling relation $\gamma_M = (D - 3)\gamma$ outlined in [103] for $D \geq 4$, adopting a modified form $\gamma_M = 2\gamma$. This requires further investigation.

Appendix D: Hoop conjecture

Thorne’s hoop conjecture [88] postulates that a mass \mathcal{M} collapses to form a BH if and only if it can be enclosed by a circular hoop of critical circumference $C_{critical} = 4\pi\mathcal{M}$ [89–91]. This implies $C \leq 4\pi\mathcal{M}$ for BH formation.

We explore this conjecture within the percolation model, associating the the length of the smallest percolation cluster with the circumference C , and the energy of the smallest cluster in the percolation model will be identified with the mass \mathcal{M} specified by the hoop conjecture. The length of the smallest cluster is defined as the number of distinct states within the cluster, while the energy of the smallest cluster corresponds to the number of connected bonds it contains.

Figure 5 is the plot of the number of connected bonds, E_b , and the number of states C in the smallest cluster for both NN (red) and NNN (blue) dominated phases. The red and blue dots refer to the numerical output for different lattice sizes $3 \leq N \leq 20$. The results reveal that the slopes of the plotted lines for both the NN and NNN dominating phases are equal. The equal slopes suggest $\mathcal{U} \geq 1$ (NN) and $v \geq 1$ (NNN), but these do not necessarily imply $v \geq \mathcal{U}$, a BH formation requirement. Thus, the conjecture does not favor one phase over the other.

While the hoop conjecture holds in both phases, BH formation occurs only in the NNN phase. This is due to the exponential growth of both cluster number and energy in the NNN phase, facilitating gravitational collapse. The NN phase exhibits only linear growth, preventing BH formation.

-
- [1] Roger Penrose, “Gravitational collapse and space-time singularities,” *Phys. Rev. Lett.* **14**, 57–59 (1965).
- [2] S. W. Hawking, “Particle Creation by Black Holes,” *Commun. Math. Phys.* **43**, 199–220 (1975), [Erratum: *Commun.Math.Phys.* 46, 206 (1976)].

- [3] S. W. Hawking, “Breakdown of predictability in gravitational collapse,” *Phys. Rev. D* **14**, 2460–2473 (1976).
- [4] José M. M. Senovilla and David Garfinkle, “The 1965 Penrose singularity theorem,” *Class. Quant. Grav.* **32**, 124008 (2015), [arXiv:1410.5226 \[gr-qc\]](#).
- [5] John Preskill, “Do black holes destroy information,” in *Proceedings of the International Symposium on Black Holes, Membranes, Wormholes and Superstrings*, S. Kalara and DV Nanopoulos, (World Scientific, 1992) pp. 22–39.
- [6] D. Harlow, “Jerusalem lectures on black holes and quantum information,” *Rev. Mod. Phys.* **88**, 015002 (2016).
- [7] Donald Marolf, “The Black Hole information problem: past, present, and future,” *Rept. Prog. Phys.* **80**, 092001 (2017), [arXiv:1703.02143 \[gr-qc\]](#).
- [8] William Ballik and Kayll Lake, “Vector volume and black holes,” *Phys. Rev. D* **88**, 104038 (2013), [arXiv:1310.1935 \[gr-qc\]](#).
- [9] Pisin Chen, Yen Chin Ong, and Dong-han Yeom, “Black Hole Remnants and the Information Loss Paradox,” *Phys. Rept.* **603**, 1–45 (2015), [arXiv:1412.8366 \[gr-qc\]](#).
- [10] Marios Christodoulou and Carlo Rovelli, “How big is a black hole?” *Phys. Rev. D* **91**, 064046 (2015), [arXiv:1411.2854 \[gr-qc\]](#).
- [11] Ingemar Bengtsson and Emma Jakobsson, “Black holes: Their large interiors,” *Mod. Phys. Lett. A* **30**, 1550103 (2015), [arXiv:1502.01907 \[gr-qc\]](#).
- [12] Fabio D’Ambrosio, Marios Christodoulou, Pierre Martin-Dussaud, Carlo Rovelli, and Farshid Soltani, “End of a black hole’s evaporation,” *Phys. Rev. D* **103**, 106014 (2021), [arXiv:2009.05016 \[gr-qc\]](#).
- [13] R. Penrose, “Gravitational collapse: The role of general relativity,” *Riv. Nuovo Cim.* **1**, 252–276 (1969).
- [14] S. Shankaranarayanan and Joseph P. Johnson, “Modified theories of gravity: Why, how and what?” *Gen. Rel. Grav.* **54**, 44 (2022), [arXiv:2204.06533 \[gr-qc\]](#).
- [15] Abhay Ashtekar, Frans Pretorius, and Fethi M. Ramazanoglu, “Evaporation of 2-Dimensional Black Holes,” *Phys. Rev. D* **83**, 044040 (2011), [arXiv:1012.0077 \[gr-qc\]](#).
- [16] Abhay Ashtekar, Frans Pretorius, and Fethi M. Ramazanoglu, “Surprises in the Evaporation of 2-Dimensional Black Holes,” *Phys. Rev. Lett.* **106**, 161303 (2011), [arXiv:1011.6442 \[gr-qc\]](#).
- [17] Elias Okon and Daniel Sudarsky, “The Black Hole Information Paradox and the Collapse of

- the Wave Function,” *Found. Phys.* **45**, 461–470 (2015), [arXiv:1406.2011 \[gr-qc\]](#).
- [18] Susobhan Mandal, Tausif Parvez, and S. Shankaranarayanan, “From the Horndeski action to the Callan-Giddings-Harvey-Strominger model and beyond,” *Phys. Rev. D* **109**, L041502 (2024), [arXiv:2311.07921 \[gr-qc\]](#).
- [19] Ralf Schutzhold and William G. Unruh, “Gravity wave analogs of black holes,” *Phys. Rev. D* **66**, 044019 (2002), [arXiv:gr-qc/0205099](#).
- [20] W. G. Unruh and R. Schutzhold, “On slow light as a black hole analog,” *Phys. Rev. D* **68**, 024008 (2003), [arXiv:gr-qc/0303028](#).
- [21] W. G. Unruh, “Dumb holes: Analogues for black holes,” *Phil. Trans. Roy. Soc. Lond. A* **366**, 2905–2913 (2008).
- [22] Subir Sachdev, “Holographic metals and the fractionalized Fermi liquid,” *Phys. Rev. Lett.* **105**, 151602 (2010), [arXiv:1006.3794 \[hep-th\]](#).
- [23] Subir Sachdev, “Bekenstein-Hawking Entropy and Strange Metals,” *Phys. Rev. X* **5**, 041025 (2015), [arXiv:1506.05111 \[hep-th\]](#).
- [24] Subir Sachdev, “Quantum statistical mechanics of the Sachdev-Ye-Kitaev model and charged black holes,” *Int. J. Mod. Phys. B* **38**, 2430003 (2024), [arXiv:2304.13744 \[cond-mat.str-el\]](#).
- [25] Subir Sachdev, “Strange metals and black holes: insights from the Sachdev-Ye-Kitaev model,” *Oxford Research Encyclopedia of Physics* (2023), [10.1093/acrefore/9780190871994.013.48](#), [arXiv:2305.01001 \[cond-mat.str-el\]](#).
- [26] Yun-Hao Shi *et al.*, “Quantum simulation of Hawking radiation and curved spacetime with a superconducting on-chip black hole,” *Nature Commun.* **14**, 3263 (2023), [arXiv:2111.11092 \[quant-ph\]](#).
- [27] D. I. Pikulin and M. Franz, “Black hole on a chip: Proposal for a physical realization of the sachdev-ye-kitaev model in a solid-state system,” *Phys. Rev. X* **7**, 031006 (2017).
- [28] J. S. Pedernales, M. Beau, S. M. Pittman, I. L. Egusquiza, L. Lamata, E. Solano, and A. del Campo, “Dirac equation in $(1+1)$ -dimensional curved spacetime and the multiphoton quantum rabi model,” *Phys. Rev. Lett.* **120**, 160403 (2018).
- [29] Viktor Könye, Corentin Morice, Dmitry Chernyavsky, Ali G. Moghaddam, Jeroen van den Brink, and Jasper van Wezel, “Horizon physics of quasi-one-dimensional tilted weyl cones on a lattice,” *Phys. Rev. Res.* **4**, 033237 (2022).
- [30] S. Giovanazzi, “Hawking radiation in sonic black holes,” *Phys. Rev. Lett.* **94**, 061302 (2005).

- [31] Daan Maertens, Nick Bultinck, and Karel Van Acoleyen, “Hawking radiation on the lattice from floquet and local hamiltonian quench dynamics,” *Phys. Rev. B* **109**, 014309 (2024).
- [32] T. A. Jacobson and G. E. Volovik, “Effective space-time and Hawking radiation from moving domain wall in thin film of He-3-A,” *JETP Lett.* **68**, 874–880 (1998), [arXiv:gr-qc/9811014](#).
- [33] Pritam Banerjee, Suvankar Paul, and Tapobrata Sarkar, “Curvature couplings of massless fermions in analog gravity,” *Phys. Lett. B* **789**, 160–166 (2019).
- [34] Kunal Pal, Kuntal Pal, and Tapobrata Sarkar, “Analogue Metric in a Black-Bounce Background,” *Universe* **8**, 197 (2022), [arXiv:2204.06395 \[gr-qc\]](#).
- [35] S. W. Hawking and Don N. Page, “Thermodynamics of Black Holes in anti-De Sitter Space,” *Commun. Math. Phys.* **87**, 577 (1983).
- [36] Andrew Chamblin, Roberto Emparan, Clifford V. Johnson, and Robert C. Myers, “Charged AdS black holes and catastrophic holography,” *Phys. Rev. D* **60**, 064018 (1999), [arXiv:hep-th/9902170](#).
- [37] Andrew Chamblin, Roberto Emparan, Clifford V. Johnson, and Robert C. Myers, “Holography, thermodynamics and fluctuations of charged AdS black holes,” *Phys. Rev. D* **60**, 104026 (1999), [arXiv:hep-th/9904197](#).
- [38] Reevu Maity, Pratim Roy, and Tapobrata Sarkar, “Black Hole Phase Transitions and the Chemical Potential,” *Phys. Lett. B* **765**, 386–394 (2017), [arXiv:1512.05541 \[hep-th\]](#).
- [39] C. Fairoos, “Topological interpretation of black hole phase transition in Gauss–Bonnet gravity,” *Int. J. Mod. Phys. A* **39**, 2450030 (2024), [arXiv:2311.04050 \[gr-qc\]](#).
- [40] Zhong-Ying Fan, “Topological interpretation for phase transitions of black holes,” *Phys. Rev. D* **107**, 044026 (2023), [arXiv:2211.12957 \[gr-qc\]](#).
- [41] Pavan Kumar Yerra, Chandrasekhar Bhamidipati, and Sudipta Mukherji, “Topology of critical points and Hawking-Page transition,” *Phys. Rev. D* **106**, 064059 (2022), [arXiv:2208.06388 \[hep-th\]](#).
- [42] Subir Sachdev and Jinwu Ye, “Gapless spin fluid ground state in a random, quantum Heisenberg magnet,” *Phys. Rev. Lett.* **70**, 3339 (1993), [arXiv:cond-mat/9212030](#).
- [43] Jonathan Oppenheim, “Thermodynamics with long-range interactions: From ising models to black holes,” *Phys. Rev. E* **68**, 016108 (2003).
- [44] Mustafa Saeed and Viqar Husain, “Ising-like models on Euclidean black holes,” *Class. Quant. Grav.* **41**, 015002 (2024), [arXiv:2306.08547 \[gr-qc\]](#).

- [45] Ted Jacobson and David Mattingly, “Hawking radiation on a falling lattice,” *Phys. Rev. D* **61**, 024017 (1999).
- [46] W. G. Unruh, “Experimental black-hole evaporation?” *Phys. Rev. Lett.* **46**, 1351–1353 (1981).
- [47] Carlos Barcelo, Stefano Liberati, and Matt Visser, “Analogue gravity,” *Living Rev. Rel.* **14**, 3 (2011), [arXiv:gr-qc/0505065](#).
- [48] Yuval Rosenberg, “Optical analogues of black-hole horizons,” *Phil. Trans. Roy. Soc. Lond. A* **378**, 20190232 (2020), [arXiv:2002.04216 \[physics.optics\]](#).
- [49] Samuel L. Braunstein, Stefano Pirandola, and Karol Życzkowski, “Better late than never: Information retrieval from black holes,” *Phys. Rev. Lett.* **110**, 101301 (2013).
- [50] Christopher R. Stephens, Gerard ’t Hooft, and Bernard F. Whiting, “Black hole evaporation without information loss,” *Class. Quant. Grav.* **11**, 621–648 (1994), [arXiv:gr-qc/9310006](#).
- [51] Saurya Das, S. Shankaranarayanan, and Sourav Sur, “Black hole entropy from entanglement: A Review,” (2008), [arXiv:0806.0402 \[gr-qc\]](#).
- [52] Maciej Lewenstein, Anna Sanpera, Veronica Ahufinger, Bogdan Damski, Aditi Sen(De), and Ujjwal Sen, “Ultracold atomic gases in optical lattices: mimicking condensed matter physics and beyond,” *Advances in Physics* **56**, 243–379 (2007).
- [53] Juan Ramón Muñoz de Nova, Katrine Golubkov, Victor I. Kolobov, and Jeff Steinhauer, “Observation of thermal Hawking radiation and its temperature in an analogue black hole,” *Nature* **569**, 688–691 (2019), [arXiv:1809.00913 \[gr-qc\]](#).
- [54] Jeff Steinhauer, Murad Abuzarli, Tangui Aladjidi, Tom Bienaimé, Clara Piekarski, Wei Liu, Elisabeth Giacobino, Alberto Bramati, and Quentin Glorieux, “Analogue cosmological particle creation in an ultracold quantum fluid of light,” *Nature Commun.* **13**, 2890 (2022), [arXiv:2102.08279 \[cond-mat.quant-gas\]](#).
- [55] Lotte Mertens, Ali G. Moghaddam, Dmitry Chernyavsky, Corentin Morice, Jeroen van den Brink, and Jasper van Wezel, “Thermalization by a synthetic horizon,” *Phys. Rev. Res.* **4**, 043084 (2022), [arXiv:2206.08041 \[cond-mat.str-el\]](#).
- [56] Thomas G. Philbin, Chris Kuklewicz, Scott Robertson, Stephen Hill, Friedrich König, and Ulf Leonhardt, “Fiber-optical analog of the event horizon,” *Science* **319**, 1367–1370 (2008).
- [57] Jiayue Yang, Niayesh Afshordi, Mahdi Torabian, Seyed Akbar Jafari, and G. Baskaran, “Smart Holes: Analogue black holes with the right temperature and entropy,” (2024),

- [arXiv:2412.08517 \[hep-th\]](#).
- [58] Xia Wang, Changjiang Yi, and Claudia Felser, “Chiral quantum materials: When chemistry meets physics,” *Advanced Materials* **36**, 2308746 (2024).
- [59] M. Z. Hasan and C. L. Kane, “Topological Insulators,” *Rev. Mod. Phys.* **82**, 3045 (2010), [arXiv:1002.3895 \[cond-mat.mes-hall\]](#).
- [60] B. Andrei Bernevig and Taylor L. Hughes, *Topological insulators and topological superconductors* (Princeton University Press, 2013).
- [61] Dmitri E. Kharzeev, “The Chiral Magnetic Effect and Anomaly-Induced Transport,” *Prog. Part. Nucl. Phys.* **75**, 133–151 (2014), [arXiv:1312.3348 \[hep-ph\]](#).
- [62] N. Craig *et al.*, “Snowmass Theory Frontier Report,” (2022), [arXiv:2211.05772 \[hep-ph\]](#).
- [63] Zohreh Davoudi *et al.*, “Report of the Snowmass 2021 Topical Group on Lattice Gauge Theory,” in *Snowmass 2021* (2022) [arXiv:2209.10758 \[hep-lat\]](#).
- [64] Holger Bech Nielsen and M. Ninomiya, “No Go Theorem for Regularizing Chiral Fermions,” *Phys. Lett. B* **105**, 219–223 (1981).
- [65] O. M. Sotnikov, V. V. Mazurenko, J. Colbois, F. Mila, M. I. Katsnelson, and E. A. Stepanov, “Probing the topology of the quantum analog of a classical skyrmion,” *Phys. Rev. B* **103**, L060404 (2021).
- [66] Ewan Forbes, Matthew D. Horner, Andrew Hallam, Joseph Barker, and Jiannis K. Pachos, “Exploring interacting chiral spin chains in terms of black hole physics,” *Phys. Rev. B* **108**, 245142 (2023).
- [67] Matthew D. Horner, Andrew Hallam, and Jiannis K. Pachos, “Chiral Spin-Chain Interfaces Exhibiting Event-Horizon Physics,” *Phys. Rev. Lett.* **130**, 016701 (2023), [arXiv:2207.08840 \[cond-mat.str-el\]](#).
- [68] Matthew W. Choptuik, “Universality and scaling in gravitational collapse of a massless scalar field,” *Phys. Rev. Lett.* **70**, 9–12 (1993).
- [69] Dietrich Stauffer and Amnon Aharony, *Introduction to percolation theory* (Taylor & Francis, 2018).
- [70] D. Stauffer, “Scaling theory of percolation clusters,” *Physics Reports* **54**, 1–74 (1979).
- [71] Dimitris I. Tsomokos, Juan José García-Ripoll, Nigel R. Cooper, and Jiannis K. Pachos, “Chiral entanglement in triangular lattice models,” *Phys. Rev. A* **77**, 012106 (2008).
- [72] Christian D’Cruz and Jiannis K. Pachos, “Chiral phase from three-spin interactions in an

- optical lattice,” *Phys. Rev. A* **72**, 043608 (2005).
- [73] Jiayue Yang, Niayesh Afshordi, Mahdi Torabian, Seyed Akbar Jafari, and G. Baskaran, “Smart Holes: Analogue black holes with the right temperature and entropy,” (2024), [arXiv:2412.08517 \[hep-th\]](#).
- [74] Aiden Daniel, Andrew Hallam, Matthew D. Horner, and Jiannis K. Pachos, “Optimally scrambling chiral spin-chain with effective black hole geometry,” (2024), [arXiv:2404.14473 \[cond-mat.str-el\]](#).
- [75] S. Mahesh Chandran and S. Shankaranarayanan, “One-to-one correspondence between entanglement mechanics and black hole thermodynamics,” *Phys. Rev. D* **102**, 125025 (2020), [arXiv:2010.03418 \[gr-qc\]](#).
- [76] Pascual Jordan and Eugene P. Wigner, “About the Pauli exclusion principle,” *Z. Phys.* **47**, 631–651 (1928).
- [77] SHI-JIAN Gu, “Fidelity approach to quantum phase transitions,” *Int. J. Mod. Phys. B* **24**, 4371–4458 (2010).
- [78] S. Shankaranarayanan, “Temperature and entropy of Schwarzschild-de Sitter space-time,” *Phys. Rev. D* **67**, 084026 (2003), [arXiv:gr-qc/0301090](#).
- [79] Hans Reissner, “Über die eigengravitation des elektrischen feldes nach der einsteinschen theorie,” *Annalen der Physik* **355**, 106–120 (1916).
- [80] Gunnar Nordström, “On the energy of the gravitation field in einstein’s theory,” *Koninklijke Nederlandse Akademie van Wetenschappen Proceedings Series B Physical Sciences* **20**, 1238–1245 (1918).
- [81] K. Kieling and J. Eisert, “Percolation in quantum computation and,” in *Quantum and Semi-classical Percolation and Breakdown in Disordered Solids*, edited by Bikas K. Chakrabarti, Kamal K. Bardhan, and Asok K. Sen (Springer Berlin Heidelberg, Berlin, Heidelberg, 2009) pp. 1–33.
- [82] Sthitadhi Roy, David E. Logan, and J. T. Chalker, “Exact solution of a percolation analog for the many-body localization transition,” *Phys. Rev. B* **99**, 220201 (2019).
- [83] Sthitadhi Roy, J. T. Chalker, and David E. Logan, “Percolation in fock space as a proxy for many-body localization,” *Phys. Rev. B* **99**, 104206 (2019).
- [84] Staszek Welsh and David E Logan, “Simple probability distributions on a fock-space lattice,” *Journal of Physics: Condensed Matter* **30**, 405601 (2018).

- [85] David E. Logan and Staszek Welsh, “Many-body localization in fock space: A local perspective,” [Phys. Rev. B **99**, 045131 \(2019\)](#).
- [86] K. J. Schrenk, N. Posé, J. J. Kranz, L. V. M. van Kessenich, N. A. M. Araújo, and H. J. Herrmann, “Percolation with long-range correlated disorder,” [Phys. Rev. E **88**, 052102 \(2013\)](#).
- [87] Sona Prakash, Shlomo Havlin, Moshe Schwartz, and H. Eugene Stanley, “Structural and dynamical properties of long-range correlated percolation,” [Phys. Rev. A **46**, R1724–R1727 \(1992\)](#).
- [88] Kip S Thorne, Charles W Misner, and John Archibald Wheeler, *Gravitation* (Freeman San Francisco, 2000).
- [89] Eanna Flanagan, “Hoop conjecture for black-hole horizon formation,” [Phys. Rev. D **44**, 2409–2420 \(1991\)](#).
- [90] Shahar Hod, “On the status of the hoop conjecture in charged curved spacetimes,” [Eur. Phys. J. C **78**, 1013 \(2018\)](#), [arXiv:1903.09786 \[gr-qc\]](#).
- [91] W.B. Bonnor, “The hoop conjecture on black holes,” [Phys. Lett. A **99**, 424–426 \(1983\)](#).
- [92] Shahar Hod, “Further evidence for the non-existence of a unified hoop conjecture,” [Eur. Phys. J. C **80**, 982 \(2020\)](#), [arXiv:2012.08352 \[gr-qc\]](#).
- [93] Sharon M. Morsink and Robert B. Mann, “Black hole radiation of Dirac particles in (1+1)-dimensions,” [Class. Quant. Grav. **8**, 2257–2268 \(1991\)](#).
- [94] Run-Qiu Yang, Hui Liu, Shining Zhu, Le Luo, and Rong-Gen Cai, “Simulating quantum field theory in curved spacetime with quantum many-body systems,” [Phys. Rev. Res. **2**, 023107 \(2020\)](#).
- [95] Arjun Bagchi, Aritra Banerjee, Rudranil Basu, Minhajul Islam, and Saikat Mondal, “Magic fermions: Carroll and flat bands,” [JHEP **03**, 227 \(2023\)](#), [arXiv:2211.11640 \[hep-th\]](#).
- [96] Aritra Banerjee, Sudipta Dutta, and Saikat Mondal, “Carroll fermions in two dimensions,” [Phys. Rev. D **107**, 125020 \(2023\)](#), [arXiv:2211.11639 \[hep-th\]](#).
- [97] Tevian Dray and Gerard 't Hooft, “The Gravitational Shock Wave of a Massless Particle,” [Nucl. Phys. B **253**, 173–188 \(1985\)](#).
- [98] Manu Srivastava and S. Shankaranarayanan, “Non-trivial quantum fluctuations in asymptotically non-flat black-hole space-times,” [Annals Phys. **440**, 168829 \(2022\)](#), [arXiv:2008.00429 \[gr-qc\]](#).
- [99] Kris Mackewicz and Craig Hogan, “Gravity of two photon decay and its quantum coherence,”

- [Class. Quant. Grav.](#) **39**, 075015 (2022), [arXiv:2108.03264 \[gr-qc\]](#).
- [100] David Garfinkle and G. Comer Duncan, “Scaling of curvature in subcritical gravitational collapse,” [Phys. Rev. D](#) **58**, 064024 (1998).
- [101] Carsten Gundlach and Jose M Martin-Garcia, “Critical phenomena in gravitational collapse,” [Living Reviews in Relativity](#) **10**, 1–57 (2007).
- [102] Demetrios Christodoulou, “The formation of black holes and singularities in spherically symmetric gravitational collapse,” [Commun. Pure Appl. Math.](#) **44**, 339–373 (1991).
- [103] Evgeny Sorkin and Yonatan Oren, “Choptuik’s scaling in higher dimensions,” [Phys. Rev. D](#) **71**, 124005 (2005).
- [104] Sean M Carroll, *Spacetime and geometry* (Cambridge University Press, 2019).
- [105] Yoav Peleg, Sukanta Bose, and Leonard Parker, “Choptuik scaling and quantum effects in 2d dilaton gravity,” [Phys. Rev. D](#) **55**, R4525–R4528 (1997).